Original Manuscript

Title: Electrical Fields Induced Inside the Rat Brain with Skin, Skull, and Dural Placements of the Current Injection Electrode

Ahmet S. Asan, MS
Department of Biomedical Engineering
New Jersey Institute of Technology
University Heights
Newark, NJ 07102 USA

Sinan Gok, PhD
Department of Biomedical Engineering
New Jersey Institute of Technology
University Heights
Newark, NJ 07102 USA

Mesut Sahin, PhD
Professor of Biomedical Engineering
Associate Editor, IEEEE Tran. on Biomedical Circuits and Systems
Department of Biomedical Engineering
New Jersey Institute of Technology
University Heights
Newark, NJ 07102 USA
Web: http://web.njit.edu/~sahin
Email: sahin@njit.edu

Corresponding author: Mesut Sahin, PhD

Author contributions: Ahmet S. Asan contributed to experimental design, collected the data, and performed signal analysis. Sinan Gok was involved in data collection and drafting the manuscript. Mesut Sahin conceived and designed the experiments, interpreted the data, and reviewed the manuscript.

Abstract

Transcranial electrical stimulation (tES) is rapidly becoming an indispensable clinical tool with its different forms. Animal data are crucially needed for better understanding of the underlying mechanisms of tES. For reproducibility of results in animal experiments, the electric fields inside the brain parenchyma induced by the injected currents need to be predicted accurately. In this study, we measured the electrical fields in the rat brain perpendicular to the brain surface when the stimulation electrode was placed over the skin, skull, or dura mater through a craniotomy hole. The E-field attenuation through the skin was a few times larger than that of the skull. The E-field declined much faster in the gray matter underneath the pial surface than it did in the white matter, and thus the large E-fields were contained mostly in the gray matter. The transition at the gray/white matter border caused a significant peak in the E-field, as well as any other local inhomogeneties. The vertical E-field near the cortex is about one third of what is estimated by analytical solutions for volume conductors that assume a semi-infinite homogenous medium for the brain and a conductivity value of 0.2 S/m. A global scaling factor of 1/3 can be useful to account for deviations from the analytical equations in rat experiments and for more realistic estimations of the E-field peak underneath the electrode. Finally, insertion of the current return electrode into the shoulder, submandibular, and hind leg muscles had virtually no effects on the measured E-field amplitudes in the cortex underneath the epidural electrodes.

Keywords: transcranial electrical stimulation, electrical field distribution, volume conductor

I. INTRODUCTION

Transcranial electrical stimulation (tES) has emerged as an effective non-invasive technique for modulation of the brain activity in recent years, while the earliest studies date back more than a century (1). In general, the safety of the tES and its derivations has now been agreed upon so long as the current is kept below 2mA, although recent reports seem to suggest 4mA as the limit (2). These tES derivations include transcranial direct current stimulation (tDCS), transcranial alternating current stimulation (tACS), and transcranial random noise stimulation (tRNS) (3). Despite widespread interest in clinical applications, the exact mechanisms of action for tES are still being investigated.

Aforementioned tES techniques inject weak electrical currents through the brain and presumably cause only subthreshold modulation of the neuronal membrane potentials (4). Early animal studies demonstrated that neuronal firing rates could be modulated by applying direct currents (DC) to the brain (5,6) and the modulatory effects of transcranial DC electric fields were confirmed in human studies (7,8). While the excitatory and inhibitory effects of tDCS are attributed to the direction of the applied current on a larger scale (anodal vs. cathodal) (6,7,9), a more detailed analysis revealed that the primary factor is the position and orientation of the individual neuronal structures relative to the electric field. *In vitro* measurements on rat hippocampal slices showed that the amplitude and delay of the population spikes evoked by orthodromic stimulation were affected linearly by the applied uniform electric fields (10). Furthermore, even small electric fields induced polarization of CA1 pyramidal cells of the hippocampus when applied parallel to the somato-dendritic axis, but failed to do so when applied perpendicularly. Studies on the rat motor cortex slices indicated that somatic polarization was also correlated with the neuronal morphology, and the layer V pyramidal cells were the most sensitive to subthreshold electric fields (11). In general it seems that a realistic estimation of the electric field distribution inside the brain parenchyma is needed as a starting point for accurate interpretations of the neurological impact of the intervention.

70 The electric field can be controlled by adjusting the stimulation/charge intensity and steered to
71 a certain extent by careful positioning of the extracranial electrodes. Nevertheless, the electrical
72 properties of different tissues that the current passes through play a significant role in distribution of
73 the electric field. Direct *in vivo* measurement of the electric field in human subjects is not an option from
74 a clinical standpoint, thus most investigators resort to computational models in order to approximate
75 the electric field distribution in the human brain under varying stimulation intensities and electrode
76 arrangements. Miranda *et al.* used a spherical head model and estimated that almost 50% of the
77 injected current is shunted through the scalp (12). Datta *et al*. used a more advanced head model where
78 gyri/sulci specificity was defined and predicted that the electric field was concentrated at distinct sites,
79 like the walls of the gyri (13). In summary, tES induced current flow is a complex phenomenon that is
80 influenced by several factors including: 1) skull and scalp thicknesses and their compositions, 2) CSF
81 thickness and conductivity, 3) gyri/sulci morphology, 4) electrode size and geometry, and 5) positioning
82 of the stimulating and return electrodes (13,14).

83 In addition to human computational models, tES effects have been studied in animals where the
84 main interests are understanding the underlying cellular and molecular mechanisms, optimizing
85 stimulation protocols, and establishing safety limits. To this end, animal models provide ample
86 opportunities to rapidly develop new tDCS methodologies and measure the outcomes while
87 manipulating the stimulation parameters within a wide range (see (15) for a review). For accurate
88 interpretation of the results from these animal studies, realistic estimates of the induced electric field
89 distribution are needed. Direct measurement of the electric fields in brain tissue goes back to as early as
90 1950s with experiments carried on anesthetized monkeys (16), nevertheless, these studies progressed
91 very slowly since then. Chan *et al.* conducted a series of experiments using isolated turtle cerebella, and
92 studied the relationship between the applied fields and the spontaneous neuronal activity (17,18). More

recent studies on monkeys (19) and rats (20) also reported electric field measurements, although restricted either to the cortical surface or a single horizontal plane, respectively.

The tDCS technique can benefit from *in vivo* animal data, which are clearly lacking in the literature, for better understanding of the mechanisms. While the computational models provide a basic understanding of how electrical currents are distributed through the animal brain (21) as much as the human brain, they can lead to unrealistic conclusions if they primarily depend on conductivity measurements gathered from *ex vivo* tissue samples (22). Furthermore, anatomical differences in the brain size and the skin, skull, and CSF thicknesses make it difficult to extrapolate the results of an electric field model developed for one species to another. In this study, we used a rat model to measure the intracerebral voltages at varying depths and horizontal distances from the stimulating electrode. Vertical electric fields were reported for three stimulation conditions in which the anodic electrode was placed over the shaved skin, the skull, and the dura mater. The rat brain was selected in this study due to its common usage as an animal model. We anticipate that the results of this study will provide a reference point for more realistic estimations of the electric field distribution in other studies using the rat model and help to improve the reproducibility of the reported tES effects. Some of the results, such as the shunting effect of the skin and the CSF, agree with modeling predictions, while some others such as the much smaller attenuation by the rat skull, the E-field peaks at the white/gray matter border, and insensitivity of the field to the reference electrode location are among the practical findings of this study.

II. METHODS

Animal Surgery

Nine Sprague Dawley (SD) rats (250-350g, male) were used in this study for direct measurements of the electric field distribution in the brain parenchyma. All procedures were approved and performed in

accordance with the guidelines of the Institutional Animal Care and Use Committee (IACUC), Rutgers University, Newark, NJ. Anesthesia was induced with 5% isoflurane gas in an induction chamber, maintained by 1-3% isoflurane in 95% oxygen after moving the animals to a stereotaxic frame, and monitored using the toe pinch reflex. Blood oxygen level was monitored via a pulse oximeter from the hind paw. Body temperature was measured with a rectal temperature probe and regulated with a heating pad underneath the animal over the course of surgery. The hair over the head was shaved with an electric shaver and treated with a depilatory cream to remove the fine hair. The skin was cleansed with antiseptic solution.

Current Injection over the Skin:

Either 4mm diameter pellet electrodes (EP4, Ag/AgCl, World Precision Inst., FL) or 1.5mm diameter helical wire electrodes were used to inject the electric currents. The pellet electrode was positioned such that medial edge was juxtaposed to the sagittal suture and the caudal edge to the coronal suture. For helical electrodes, a Ag/AgCl wire with 125µm uncoated thickness (A-M Systems, #786000) was wrapped around a 1.25mm diameter rod 4 times to form a helix with a large surface area and thus a lower impedance. The impedance was confirmed to be below 10kΩ @1kHz in PBS. The helical electrode was filled with conductive gel in the center to ensure good contact with the skin and distribute the current more uniformly at the base of the electrode. The helical electrode was placed with its center positioned 2mm lateral (left or right) from the sagittal suture and 2mm either rostral or caudal to the coronal suture. Another Ag/AgCl wire was inserted to the ipsilateral shoulder muscles as the return (cathodic) electrode for the injected current. Ten monophasic anodic pulses were delivered as a train at 100µA amplitude, 100ms pulse width, and a repetition rate of 4Hz. The amplitude was switched to 200µA at times to increase the signal-to-noise ratio where the recorded amplitudes were too small. In this protocol, substituting pulsed stimulation for DC allowed us to overcome the poor DC response of the metal recording electrodes.

140 A sharp cut was made into the skin with a surgical blade at the edge of the stimulation electrode
141 to expose the skull caudally while leaving the skin underneath the electrode intact (Fig. 1B). Two 1mm
142 diameter craniotomy holes were drilled 2mm and 4mm away from the caudal edge of the stimulation
143 electrode using a micro drill (OmniDrill 35, World Precision Inst., FL). A tungsten electrode (0.5 MΩ,
144 TM33B05H, World Precision Inst.) was inserted into the craniotomy hole to record the induced voltages
145 as a function of depth with respect to another Ag/AgCl reference electrode attached on the skull near
146 the recording electrode using dental acrylic. The dura was punctured with the sharp tip of the tungsten
147 electrode and the first recording was made at the level of the cortical surface (depth=0). Using a 10µ-
148 resolution micromanipulator, the tungsten electrode was advanced into the brain parenchyma in 0.2mm
149 steps until reaching 4mm depth and thereafter in 0.5mm steps up to a depth of 6mm. The procedure
150 was repeated in both craniotomy holes, at 2mm and 4mm horizontal distances from the stimulation
151 electrode. The rising and falling edges of the recorded signals were marked using an automated
152 algorithm in MATLAB (Mathworks) to quantify the induced voltage amplitudes. In some animals, this
153 procedure was repeated on the contralateral side of the brain to obtain an additional set of
154 measurements.

155 **Fig. 1:** Drawings show the three different placements of the stimulation electrode on the rat's
156 head: A) top view. The vertical cross sections of the skin and skull in B, C, and D show the placements of
157 the helical wire stimulation electrode: B) over-the-skin, C) over-the-skull, and D) over-the-dura, and the
158 craniotomy holes for E-field measurements. Tungsten recording electrodes were inserted through the
159 craniotomy holes at 0mm (for over-the-dura stimulation only), 2mm and 4mm horizontal distances from
160 the stimulation electrode

161 **Current Injection over the Skull**:

162 The skin over the top of the skull was completely removed in this step, mostly in the same animals used
163 above. After removing the periosteum, bone wax was applied to the muscles around the edges and the
164 skull sutures on top to stop bleeding. The stimulation electrode (pellet or helical wire) was placed onto
165 the skull (Fig. 1C) at the same coordinates used with over-the-skin electrodes. The voltage recordings
166 were made following the same procedure above with slight repositioning of the tungsten electrode in
167 the same craniotomy holes in order to avoid damaged tissue from the previous penetration.

168 **Current Injection over the Dura**:

169 A 2mm craniotomy hole was made at the coordinates of the stimulation electrode to inject the current
170 directly through the dura (Fig. 1D). A helical wire electrode (1.5mm diam.) was placed about 0.5mm
171 above the dura matter and anchored to the edge of the skull hole with small amounts of cyanoacrylate
172 glue and the hole was filled with normal saline. The distances between the caudal edge of the helical
173 electrode and recording holes were kept at 2mm and 4mm as before. With the use of helical electrodes,
174 an additional set of voltage recordings were made by inserting the tungsten electrode through the
175 center of the stimulation electrode (horizontal distance=0mm).

176 Finally, in order to investigate the effect of the current return electrode position, the Ag/AgCl
177 wire inserted to the ipsilateral shoulder muscles was moved to the contralateral shoulder, the hind leg,
178 and the submandibular muscles via needle insertions. The voltage measurements were repeated near
179 the cortex and at various depths with the recording electrode in the center of the helical electrode for
180 these four different positioning of the current return electrode for comparison.

181 **Data Collection and Analysis**:

182 The signal were collected in a large Faraday cage and first amplified by a gain of 100 (Model 1700, A-M
183 Systems, WA) with filters setting of 10 Hz–10 kHz, and then sampled at 25kHz through a National
184 Instruments data acquisition board (PCI 6071) controlled by custom-designed MATLAB codes. Stimulus-

185 triggered averaging (STA) was used (N=10) to suppress the background neural activity and other sources
186 of random noise. The averaged signal was further band-pass filtered in MATLAB (10-1000Hz) before
187 analyzing. Voltage transitions within 2ms window around the rising edge of the square pulses were
188 taken as the induced voltage at the corresponding depth. The first derivative of the voltage data with
189 respect to depth was computed as the electric field (E-field). All field measurements were made
190 exclusively in the vertical direction (VE-field) in this study. Horizontal E-field measurements would
191 require derivation of the voltage measurements made through different brain penetrations and lead to
192 large calculation errors due to even slight changes in the absolute value of the voltages measured, which
193 could easily occur from repositioning of the recording reference electrode between penetrations.

194 **Comparison with Theoretical Models**

195 The resistance of a monopolar disk electrode at the surface of a semi-infinite, homogeneous, and
196 isotropic medium was first derived by Newman (23) as a function of the electrode radius (*a*), and the
197 conductivity of the medium (σ). The potential at the surface is found as $Vo = I/(4\sigma a)$, where *I* is the
198 electrode current. Wiley and Webster then solved the Laplace's equation for the voltage distribution
199 inside the semi-infinite volume conductor for a similar disk electrode (24). By substituting zero for the
200 horizontal axis *r* in their equation, we find the voltage at the electrode center, which starts from *Vo* at
201 *z*=0 and declines with increasing values of the vertical axis (*z*) according to the equation
202 $(2Vo/\pi)\sin^{-1}(a/\sqrt{z^2+a^2})$. The VE-field, however, decreases as a function of $\varphi = -(2Vo/\pi)(a/z^2 +$
203 $a^2)$, which can be found easily by differentiating the voltage equation with respect to *z,* and the peak
204 value of the VE-field at the surface (*z*=0, r=0) is $\varphi = -2Vo/(\pi a)$ or $\varphi = I/(2\pi\sigma a^2)$. We fit the VE-field
205 equation to our data collected with the epidural placement of the electrode at its center while leaving
206 *Vo* as a free parameter (Fig. 2, 0mm). The *Vo* value that fits the experimental data best for r=0 was also
207 used to plot the VE-field equation at r=2mm and r=4mm from the center of the stimulation electrode in

208 Fig. 2 (2mm and 4mm). The VE-field is shown as a 2D heat plot in Fig. 3 for comparison with the
209 experimental data and will be discussed at the end.

210 **Fig. 2:** Voltage (top row) and E-field (bottom row) measurements made with epidural (as in Fig.
211 1D) placement of the Ag/AgCl helical wire stimulation electrode with 1.5 diam. Top Row Left to Right:
212 Voltage measurements made with respect to a reference on the skull and via penetrations at the center
213 (0mm), 2mm from the center, and 4mm from the center of the helical electrode. Seven sets of
214 measurements were collected in five animals. Bottom Row: The mean of the vertical E-fields calculated
215 by differentiating the voltage measurements shown in the top row for each penetration separately. The
216 shady areas indicate ± standard error. The black solid line is the VE-field predicted by the analytical
217 equation derived by Wiley & Webster (24) that provided the best fit, i.e. highest coefficient of
218 determination (R2), when V(0,0) is set to 58.33mV. For 2mm and 4mm penetrations, the analytical
219 equation was evaluated (solid black lines) using the same V(0,0) value for consistency.

220 **Fig. 3:** Vertical E-field distribution as a heat plot on a logarithmic scale; obtained by interpolating
221 the measurements (left panel) presented in Fig. 2, and predicted by the analytical equations of Wiley &
222 Webster (right panel). Depth=0 corresponds to the surface of the cortex.

223 **III. RESULTS**

224 **VE-Fields with Epidural Injection of Current**

225 The peak-to-peak voltage induced by the current pulse was measured as a function of depth down to
226 6mm from the dura surface (Fig. 2, top row) at 0mm (center of the helix), 2mm, and 4mm away
227 horizontally from the stimulation electrode (see Fig. 1). Vertical electrical fields (VE-fields) were
228 computed by differentiating the raw voltage measurements without any filtering or curve fitting, and
229 averaged across the animals (Fig. 2, bottom row). Note that the vertical offset in the voltage plots of the
230 top row do not carry any significance since they can vary between animals depending on where the

recording reference electrode is placed along the current pathways between the stimulation and the returning electrodes. The voltage curves decline faster under the stimulation electrode with maximum values underneath the dura (depth=0mm), as expected. The VE-field was also maximum under the stimulation electrode (distance=0mm, depth=0mm) near the cortex, declined exponentially, and lost more than 75% of its strength by 2mm below the stimulation electrode and further decreased down to negligible levels by 6mm. The analytical equation by Wiley and Webster (see methods) was evaluated and fit to the VE-field by using *Vo* as the free parameter. The analytical formula provided a good-fit (R^2=0.92) including the initial plateau near the cortical surface for *Vo*=58.33mV. As the recording electrode was moved horizontally to 2mm and 4mm away from the stimulation site, the VE-field decline near the surface became sharper and an elevation appeared at deeper levels, the latter of which was predicted by the analytical equation. The sharp decline was not predicted by the analytical equation since the semi-infinite model assumes a non-conductive medium above the surface and a zero vertical current at the boundary. The band of large VE-fields extending horizontally underneath the surface can also be appreciated from the heat plot of Fig. 3A. Interestingly, for all penetrations (0, 2, 4mm) there seems to be a peak in the E-field near or a little above the 2mm mark, which may indicate a sharp change in tissue conductivity, e.g. from gray matter to white matter. The analytical equations fail to predict the VE-field amplitudes, in general, at 2mm and 4mm from the stimulation electrode with the same *Vo* used at 0mm. Thus, the VE-fields expand more in the horizontal direction than predicted.

Comparison of VE-Fields with Current Injections over the Skin, Skull, and Dura

Figure 4 compares the VE-fields with three different placements of the helical electrode; over the skin, skull, and dura. The epidural stimulation produces the largest electric field intensities in the brain parenchyma while epidermal placement produces the lowest intensity, as expected, both at 2mm and 4mm horizontal locations from the electrode. Note that for over-the-skin and skull placements of the stimulation electrode the E-fields were not measurements in the center of the electrode in order not to

disturb the intactness of the skin or skull with a penetration hole. The skin attenuated the VE-field to a much larger degree than the skull, as seen with both penetrations at 2mm and 4mm horizontal locations from the edge of the stimulation electrode. The over-the-skin placement did not produce an exponentially decreasing VE-field profile by depth as the other two placements of the stimulation electrode, and the VE-fields measured at the cortical surface (depth=0) were about an order of magnitude smaller. The skin thickness was measured at the end of the experiment and found to be around 0.5mm under the stimulation electrode.

Fig. 4: Comparison of VE-fields for three different placements of the helical wire electrode over the skin, skull, and dura mater. Measurements are repeated at 2mm (left column) and 4mm (right column) horizontal distances from the helical electrode. The averages of (n) measurement sets are plotted (solid lines) and the standard errors are shown as shadings.

The VE-fields were also compared with larger Ag/AgCl pellet electrodes (diam.=4mm) placed either over the skin or skull (Fig. 5). At a horizontal distance of 2mm from the edge of the pellet electrode, the presence of skin attenuated the electric fields by 3-4 times, similar to the smaller helical electrodes, but the VE-field declined faster by depth with the pellet electrode compared to the smaller helical electrodes. This was probably because the pellet electrode had a larger diameter and the 2mm from the edge was actually further away from the electrode center compared to the helical electrodes. A sharper decline in the field with increasing horizontal distances was also observed with the helical electrode (Fig. 2). The VE-field bump around 1.5-2mm depth was observed consistently in these plots as well. For both skin and skull placements of the stimulation electrode, the measurements at 4mm were about a few times smaller than those at 2mm.

Fig. 5: Comparison of VE-fields for two different placements of the large pellet electrode; over the skin and skull. Details are same as in Fig. 4.

Location of the Current Return Electrode

Lastly, we investigated how the location of the stimulation reference electrode affects the electric field strength in one rat. In the previous experiments, a Ag/AgCl wire inserted into the ipsilateral shoulder was used as the cathode for current injection. For this experiment, three alternative sites were tested for the cathodic electrode; contralateral shoulder, the submandibular muscles, and the ipsilateral hind limb. The epidural stimulation experiments with the helical wire electrodes were repeated against these reference electrode placements and the VE-fields between the depths of 0.6-2.0mm were measured in five different craniotomy holes as the stimulus was applied through the same hole. The maximum deviation from the ipsi-shoulder measurements was less than 1% with any of the new reference points. None of the VE-field measurement sets (N=5) against the novel reference points were significantly different from that of the set against the ipsi-shoulder electrode (paired t-test, $p>0.5$).

IV. DISCUSSION

E-field Attenuation by Skin and Skull

The skin thickness changes around the head and rodents are no exception to this rule. Because of the compression we applied to hold the electrode down firmly on the skin, the skin thickness decreased under the stimulation electrode during the course of the experiment and found to be ~0.5mm at the end. Hence, we can only make general remarks about the skin effects on the E-field measurements in the face of these sources of variability. About a four-fold decrease occurred in the VE-field when the electrode was placed over the skin as opposed to the skull surface. The average skull thickness was measured to be ~0.5mm (N=5). In agreement with this data, Vöröslakos et al. reported that transcutaneous stimulation generated several-fold weaker electric fields compared to subcutaneous stimulation in rats (20). There was only a marginal loss of electric field intensities when the stimulation electrode was moved from the dural surface to the skull surface in our data.

301 With over-the-skin electrodes and 100μA current injection, the vertical electric field drops down
302 to ~1mV/mm at 2mm and 4mm from the stimulation electrode (Fig. 4). Terzulo and Bullock reported
303 that the firing frequency of neurons can be modulated by voltage gradients as low as 1mV/mm (9),
304 which is also the lower bound indicated by rodent studies (20,25). The large variability in the skin
305 thickness and the high conductivity of skin can make the results with epidermal montage highly
306 unpredictable. Therefore, placing the electrode over the skull would be a reasonable compromise to
307 mitigate the effects of current shunting by the skin and to improve the focality of stimulation, while
308 avoiding large E-field peaks as they occur with epidural stimulation.

309 We did not measure the VE-field at the electrode center with over-the-skull electrodes. The
310 epidural stimulations in Fig. 2 show the VE-field under the electrode decreases by about a factor of two
311 from the electrode center to 2mm off the center. If we can extrapolate from over-the-skull stimulations
312 in Fig. 4 at 2mm off the center, the VE-field in the electrode center should be about 20mV/mm at the
313 cortical level.

314 **Non-Homogeneity of the Brain**

315 That the skull resistivity was much higher than that of the skin and brain tissue was first demonstrated
316 by early intracerebral voltage measurement studies in human cadavers (26) and anesthetized monkeys
317 (16). Hayes predicted that the high conductivity of the skin and scalp would make the electrical fields
318 more or less uniform inside the brain. Our data with over-the-skin stimulation does not have the
319 exponentially decaying profile by depth as in over the skull and dura stimulations, and thus agrees with
320 Hayes' prediction in general. A particular aspect to note is the VE-field peak that occurred consistently at
321 around 1.5-2mm depths in most plots where the gray matter transitions into the white matter and a
322 significant change in local conductivity is expected. The lower conductivity of the white matter seems to
323 cause an elevation in the VE-field at the border of the two regions. The fact that the VE-field decline in

the gray matter is faster at 2mm and 4mm horizontal locations than at the electrode center (0mm, Fig. 2) must, however, be due to the higher conductivity of the cerebrospinal fluid near the surface, rather than the gray/white matter conductivity differences.

Electrode Size

The electrode size is the primary factor that can help focalize the induced E-field and the affected volume of tissue (27). Smaller size electrodes require less total current than larger electrodes to induce the same current density at a fixed target point in the brain (28). However the current density at the electrode surface is higher than that of the larger electrodes (29). We did not specifically compare the two different electrode sizes we had due to insufficient statistical power in the data.

Monopolar vs. Bipolar Montages

Repositioning the return electrode from the shoulder to other muscles around the body introduced changes smaller than 1% in the VE-field. This is explained by the fact that the voltage profile near the anodic electrode is more or less the same with the monopolar montage so long as the large surface return electrode is placed far enough in the body. The field steering effect begins to occur when the return electrode is brought near the stimulation electrode, hence approximating a bipolar montage. The sensitivity to the location of the return electrode may increase with epidermal placement of the anodic electrode, especially at locations further away from it.

The fact that the E-field declines sharply by distance with monopolar montages is advantageous for the spatial selectivity if the targeted neural structures are near the brain surface, but makes it difficult to achieve significant E-fields at deeper brain regions without causing extreme electric fields near the surface. Attempts to focus the electric field at subcortical brain regions using multiple electrodes will have to cope with this challenge. Horizontal E-field can be maximized using bipolar montages by placing both the cathode and the anode around the head on the sides, if the targeted

347 neural structures are inside the cortical sulci where the somato-dendritic axis of the neurons is oriented
348 horizontally. A recent paper (20) proposed both spatial focusing and time-multiplexing of the stimulus
349 currents via multiple dipoles in order to maximize the horizontal E-field at a focal point inside the brain
350 by taking advantage of the slow time constant of the cellular membranes at subthreshold potentials.
351 While the tES methods enjoy the benefits of being non-invasive, the challenge of focalization may
352 persist as the main disadvantage of the technique in the long run.

353 **Stimulation Waveform**

354 In our protocol, substituting DC with pulsed stimulation allowed us to overcome the poor DC response
355 of the tungsten recording electrodes. The brain tissue can be treated primarily as a resistive medium
356 and hence the recorded amplitudes to be independent of frequency, up to 10kHz and even higher
357 ranges (12,30) owing to the "quasi-static approximation". Thus, our amplifier's high cutoff (f_c) was set
358 to 10kHz, which has corresponding rise time of 15.9µs ($t_r = {}^{1}/_{2\pi f_c}$) for a first-order filter. We took the
359 amplitude measurements 1ms after the pulse transition, allowing several rise times for the signals to
360 stabilize while still being much shorter than the time constant imposed by the lower cutoff frequency of
361 the amplifier ($t_r = 15.9ms$, 10Hz) .

362 A sinusoidal waveform at a constant frequency (e.g. 1kHz) could also be used for the stimulus
363 current in this study instead of rectangular pulses. A stimulus waveform with a single frequency would
364 overcome the bandwidth limitations of the metal recording electrodes and the amplifier, which
365 attenuates the harmonics of a rectangular waveform to different degrees and distorts the recorded
366 waveforms. The advantage of the rectangular waveform, however, is that any disturbance to the
367 electrode tip during penetration manifests itself not only as a change in the measured amplitudes but
368 also as a distortion in the waveform, and thus alerts the experimenter about the quality of the signals.

369 With sinusoidal waveforms, only the signal amplitude would change, which would escape the attention
370 of the experimenter and lead to significant miscalculations of the E-field.

371 **Comparison with Theoretical Models**

372 Despite the fact that Wiley & Webster equation (24) assumes a homogeneous medium, and does not
373 account for the impedance of the electrode-electrolyte interface and the current redistribution across
374 the electrode surface due to amplitude and frequency dependency of the interface (31), it provides a
375 reference point for comparison. Comparison of the experimental data with the theoretical model in 2D
376 (Fig. 3) reveals some fundamental similarities but also significant differences. Both plots show that the
377 largest VE-fields occur under the electrode, but the experimental VE-field diminishes within the gray
378 matter for the most part, subsiding to negligible levels in the white matter. In the experimental data the
379 VE-field spreads more in the horizontal direction near the surface most likely due to the high
380 conductivity of the CSF, and perhaps the gray matter also. The theoretical plot assumes a non-
381 conductive medium above the brain and does not account for the presence of the skull. There are
382 clearly regions of varying conductivities in the experimental data that cause inhomogeneities in the
383 electric field. Lastly, the VE-peaks at the electrode edges that are suggested by the earlier analytical
384 models (24) were not observed in the experimental data. This may be because of the distance (~0.5mm)
385 allowed between the electrode surface and the brain cortex in our setup, or it may be explained partially
386 by the presence of the electrode-electrolyte interface as predicted by more advanced models (31).

387 **Practical Considerations**

388 The surface area of the electrode that is in contact with tissue primarily determines the E-field strength
389 in the vicinity of the electrode. Therefore, epidural placement of the stimulation electrode may lead to
390 large variations in the E-fields in the cortex depending on the exact position of the electrode. If the
391 electrode contact area with the cortex is well defined, the simple analytical equations (24) can become

392 very useful for predicting the potential and the VE-field underneath the electrode. The equation for the
393 VE-field at the surface (*z*=0, r=0) is $\varphi = -2Vo/(\pi a)$. For *Vo* value that gives the best fit with this equation
394 to our data was found to be 58.33mV. Assuming a homogenous medium, an overall conductivity value
395 of 0.57 S/m can be found by substituting this value of *Vo* into the Newman equation ($Vo = I/(4\sigma a)$),
396 which is about three times higher than the commonly used conductivity for the brain, most likely due to
397 the high conductivities of the CSF. For a known electrode diameter and current, one can use this
398 *'modified'* conductivity value to estimate the VE-field peak underneath the epidural electrodes. Having
399 an accurate prediction for the vertical E-field near the surface, where most of the cortical neurons are
400 found in an animal with a lissencephalic brain like the rat, can prove to be useful when direct
401 measurements of the field is not possible.

402 The current distribution across the disk electrodes is predicted to suffer from edge-effects by
403 earlier models (24). Inclusion of the electrode-electrolyte interface into the model produces a more
404 uniform current profile across the surface, although the effect is amplitude and frequency dependent
405 (31). The choice of the electrode material thus is crucial to minimize the electrode-electrolyte
406 impedance and improve reproducibility. In order to prevent the edge effects from influencing the E-
407 field distribution inside the brain, the stimulation electrode can be kept at a distance from the
408 superficial layers of the cortex. The skull can serve as a spacer in this case. The disk electrode can be
409 attached onto the skull at reproducible stereotaxic coordinates and the top of the electrode can be
410 covered with some nonconductive material to prevent current spreading through the skin. The skull
411 thickness at the point of electrode placement can be standardized to a degree by controlling the
412 weight/age of the animal. Alternatively, one can also make a craniotomy hole and fill it with conductive
413 gel or isotonic saline and position the stimulation electrode at a known distance above the cortex as we
414 did in this study. Because normal saline has a conductivity (1.67 S/m) that is about eight times higher
415 than that of the brain (0.2 S/m), the stimulation electrode may electrically be assumed to be on the

cortex/saline interface for practical purposes. The highly conductive saline may however be replaced with encapsulation tissue by time in chronic implants. For most reproducible results, the E-field should be measured directly inside the tissue in each animal separately if this can be done without disturbing the intactness of the neurons or the E-field itself.

V. CONCLUSIONS

This study provides experimental data as a reference point for more realistic estimates of the electric fields induced in the rat brain during tES studies. The skin attenuates the electric field much more strongly than the skull and causes the current spread more uniformly inside the skull. For focal stimulation, it may be best to place the stimulation electrode on the skull to avoid the skin effect. The electrical field perpendicular to the cortex decreases exponentially near the surface and loses most of its strength within 2mm into the brain underneath the electrode and within 1mm of depth off of the electrode edge. A 100µA current injected through a 1.5mm over-the-skull electrode is predicted to generate ~20mV/mm at the cortical surface. For epidural placements of the stimulation electrode through a craniotomy hole, a modified value of 0.57 S/m for the brain conductivity can be assumed to estimate the voltage at the cortical surface using the volume conductor equations. Significant E-field peaks occur in the brain parenchyma, most likely due to local conductivity changes, especially at the gray/white matter border. These large fluctuations in the E-field measurements by depth show that the homogeneous volume conductor assumption is too simplistic for a model to estimate the local effects of the injected currents.

ACKNOWLEDGMENTS

Supported by NIH/NINDS Grant No: R21 NS101386.

437 **REFERENCES**

438 1. Priori A. Brain polarization in humans: A reappraisal of an old tool for prolonged non-invasive
439 modulation of brain excitability [Internet]. Vol. 114, Clinical Neurophysiology. Elsevier; 2003
440 [cited 2018 May 14]. p. 589–95. Available from:
441 https://www.sciencedirect.com/science/article/pii/S1388245702004376?via%3Dihub

442 2. Chhatbar PY, Chen R, Deardorff R, Dellenbach B, Kautz SA, George MS, et al. Safety and
443 tolerability of transcranial direct current stimulation to stroke patients – A phase I current
444 escalation study. Brain Stimul [Internet]. 2017 May 1 [cited 2018 Aug 14];10(3):553–9. Available
445 from: https://www.sciencedirect.com/science/article/pii/S1935861X17306149?via%3Dihub

446 3. Bikson M, Grossman P, Thomas C, Zannou AL, Jiang J, Adnan T, et al. Safety of Transcranial Direct
447 Current Stimulation: Evidence Based Update 2016 [Internet]. Vol. 9, Brain Stimulation. Elsevier;
448 2016 [cited 2018 Feb 17]. p. 641–61. Available from: https://www-sciencedirect-
449 com.libdb.njit.edu:8443/science/article/pii/S1935861X16301401

450 4. Woods AJ, Antal A, Bikson M, Boggio PS, Brunoni AR, Celnik P, et al. A technical guide to tDCS,
451 and related non-invasive brain stimulation tools. Clin Neurophysiol [Internet]. 2016 Feb [cited
452 2018 Feb 12];127(2):1031–48. Available from: http://www.ncbi.nlm.nih.gov/pubmed/26652115

453 5. Creutzfeldt OD, Fromm GH, Kapp H. Influence of transcortical d-c currents on cortical neuronal
454 activity. Exp Neurol [Internet]. 1962 Jun 1 [cited 2018 May 24];5(6):436–52. Available from:
455 https://www.sciencedirect.com/science/article/pii/0014488662900560

456 6. Bindman LJ, Lippold OCJ, Redfearn JWT. The action of brief polarizing currents on the cerebral
457 cortex of the rat (1) during current flow and (2) in the production of long-lasting after-effects. J
458 Physiol [Internet]. 1964 Aug 1 [cited 2018 Jan 29];172(3):369–82. Available from:

459 http://www.ncbi.nlm.nih.gov/pubmed/14199369

460 7. Nitsche MA, Paulus W. Excitability changes induced in the human motor cortex by weak
461 transcranial direct current stimulation. J Physiol. 2000 Sep;527 Pt 3:633–9.

462 8. Lang N, Siebner HR, Ward NS, Lee L, Nitsche MA, Paulus W, et al. How does transcranial DC
463 stimulation of the primary motor cortex alter regional neuronal activity in the human brain? Eur J
464 Neurosci [Internet]. 2005 Jul 21 [cited 2018 Feb 12];22(2):495–504. Available from:
465 http://www.ncbi.nlm.nih.gov/pubmed/16045502

466 9. Terzuolo CA, Bullock TH. Measurement of imposed voltage gradient adequate to modulate
467 neuronal firing. Proc Natl Acad Sci U S A [Internet]. 1956 Sep 1 [cited 2018 May 14];42(9):687–94.
468 Available from: http://www.ncbi.nlm.nih.gov/pubmed/16589932

469 10. Bikson M, Inoue M, Akiyama H, Deans JK, Fox JE, Miyakawa H, et al. Effects of uniform
470 extracellular DC electric fields on excitability in rat hippocampal slices in vitro. J Physiol [Internet].
471 2004 May 1 [cited 2018 Feb 14];557(1):175–90. Available from:
472 http://doi.wiley.com/10.1113/jphysiol.2003.055772

473 11. Radman T, Ramos RL, Brumberg JC, Bikson M. Role of cortical cell type and morphology in
474 subthreshold and suprathreshold uniform electric field stimulation in vitro. Brain Stimul
475 [Internet]. 2009 Oct 1 [cited 2018 Feb 12];2(4):215–228.e3. Available from: https://www-
476 sciencedirect-com.libdb.njit.edu:8443/science/article/pii/S1935861X09000424

477 12. Miranda PC, Lomarev M, Hallett M. Modeling the current distribution during transcranial direct
478 current stimulation. Clin Neurophysiol [Internet]. 2006 Jul [cited 2018 Feb 17];117(7):1623–9.
479 Available from: https://ac-els-cdn-com.libdb.njit.edu:8443/S1388245706001726/1-s2.0-
480 S1388245706001726-main.pdf?_tid=spdf-bcaa1334-c0a1-4d41-ace8-

481 3264c5f7dbcf&acdnat=1518917934_be472fc3bac6d2140f8f7e1c73e4eb56

482 13. Datta A, Bansal V, Diaz J, Patel J, Reato D, Bikson M. Gyri-precise head model of transcranial
483 direct current stimulation: Improved spatial focality using a ring electrode versus conventional
484 rectangular pad. Brain Stimul [Internet]. 2009 Oct [cited 2018 May 29];2(4):201–207.e1. Available
485 from: http://www.ncbi.nlm.nih.gov/pubmed/20648973

486 14. Opitz A, Paulus W, Will S, Antunes A, Thielscher A. Determinants of the electric field during
487 transcranial direct current stimulation. Neuroimage. 2015 Apr;109:140–50.

488 15. Jackson MP, Rahman A, Lafon B, Kronberg G, Ling D, Parra LC, et al. Animal models of transcranial
489 direct current stimulation: Methods and mechanisms. Clin Neurophysiol [Internet]. 2016 Nov
490 [cited 2018 Feb 12];127(11):3425–54. Available from:
491 http://www.ncbi.nlm.nih.gov/pubmed/27693941

492 16. Hayes KJ. The current path in electric convulsion shock. Arch Neurol Psychiatry [Internet]. 1950
493 Jan 1 [cited 2018 Feb 20];63(1):102–9. Available from:
494 http://archneurpsyc.jamanetwork.com/article.aspx?doi=10.1001/archneurpsyc.1950.02310190108008

496 17. Chan CY, Nicholson C. Modulation by applied electric fields of Purkinje and stellate cell activity in
497 the isolated turtle cerebellum. J Physiol [Internet]. 1986 Feb [cited 2018 Jun 8];371:89–114.
498 Available from: http://www.ncbi.nlm.nih.gov/pubmed/3701658

499 18. Chan CY, Hounsgaard J, Nicholson C. Effects of electric fields on transmembrane potential and
500 excitability of turtle cerebellar Purkinje cells in vitro. J Physiol [Internet]. 1988 Aug [cited 2018
501 Jun 8];402:751–71. Available from: http://www.ncbi.nlm.nih.gov/pubmed/3236254

502 19. Opitz A, Falchier A, Yan C-G, Yeagle EM, Linn GS, Megevand P, et al. Spatiotemporal structure of

503 intracranial electric fields induced by transcranial electric stimulation in humans and nonhuman
504 primates. Sci Rep [Internet]. 2016 Nov 18 [cited 2018 Jan 29];6(1):31236. Available from:
505 http://www.nature.com/articles/srep31236

506 20. Vöröslakos M, Takeuchi Y, Brinyiczki K, Zombori T, Oliva A, Fernández-Ruiz A, et al. Direct effects
507 of transcranial electric stimulation on brain circuits in rats and humans. Nat Commun [Internet].
508 2018 Dec 2 [cited 2018 Apr 14];9(1):483. Available from:
509 http://www.nature.com/articles/s41467-018-02928-3

510 21. Gasca F, Marshall L, Binder S, Schlaefer A, Hofmann UG, Schweikard A. Finite element simulation
511 of transcranial current stimulation in realistic rat head model. In: 2011 5th International
512 IEEE/EMBS Conference on Neural Engineering [Internet]. IEEE; 2011 [cited 2018 Jun 25]. p. 36–9.
513 Available from: http://ieeexplore.ieee.org/document/5910483/

514 22. Huang Y, Liu AA, Lafon B, Friedman D, Dayan M, Wang X, et al. Measurements and models of
515 electric fields in the in vivo human brain during transcranial electric stimulation. Elife [Internet].
516 2017 Feb 7 [cited 2018 May 8];6:e18834. Available from: https://elifesciences.org/articles/18834

517 23. Newman J. Resistance for Flow of Current to a Disk. J Electrochem Soc [Internet]. 1966 May 1
518 [cited 2018 Aug 14];113(5):501. Available from: http://jes.ecsdl.org/cgi/doi/10.1149/1.2424003

519 24. Wiley JD, Webster JG. Analysis and control of the current distribution under circular dispersive
520 electrodes. IEEE Trans Biomed Eng [Internet]. 1982 May [cited 2018 Jun 21];29(5):381–5.
521 Available from: http://ieeexplore.ieee.org/document/4121424/

522 25. Ozen S, Sirota A, Belluscio MA, Anastassiou CA, Stark E, Koch C, et al. Transcranial electric
523 stimulation entrains cortical neuronal populations in rats. J Neurosci [Internet]. 2010 Aug 25
524 [cited 2018 Jan 29];30(34):11476–85. Available from:

525 http://www.ncbi.nlm.nih.gov/pubmed/20739569

526 26. Smitt JW, Wegener CF. ON ELECTRIC CONVULSIVE THERAPY: with particular regard to a parietal
527 application of electrodes, controlled by intracerebral voltage measurements1. Acta Psychiatr
528 Scand [Internet]. 1944 Dec 31 [cited 2018 Jun 1];19(3–4):529–49. Available from:
529 http://doi.wiley.com/10.1111/j.1600-0447.1944.tb04586.x

530 27. Nitsche MA, Doemkes S, Karakose T, Antal A, Liebetanz D, Lang N, et al. Shaping the Effects of
531 Transcranial Direct Current Stimulation of the Human Motor Cortex. J Neurophysiol [Internet].
532 2007 Apr [cited 2018 Jun 25];97(4):3109–17. Available from:
533 http://www.physiology.org/doi/10.1152/jn.01312.2006

534 28. Faria P, Hallett M, Miranda PC. A finite element analysis of the effect of electrode area and inter-
535 electrode distance on the spatial distribution of the current density in tDCS. J Neural Eng
536 [Internet]. 2011 Dec 1 [cited 2018 Jun 25];8(6):066017. Available from:
537 http://stacks.iop.org/1741-
538 2552/8/i=6/a=066017?key=crossref.83f3d9681922067b4b8b72fa29d78dd5

539 29. Miranda PC, Faria P, Hallett M. What does the ratio of injected current to electrode area tell us
540 about current density in the brain during tDCS? Clin Neurophysiol [Internet]. 2009 Jun 1 [cited
541 2018 May 14];120(6):1183–7. Available from:
542 https://www.sciencedirect.com/science/article/pii/S1388245709003046?via%3Dihub

543 30. Ruffini G, Wendling F, Merlet I, Molaee-Ardekani B, Mekonnen A, Salvador R, et al. Transcranial
544 current brain stimulation (tCS): models and technologies. IEEE Trans Neural Syst Rehabil Eng
545 [Internet]. 2013 May [cited 2018 May 8];21(3):333–45. Available from:
546 http://ieeexplore.ieee.org/document/6290404/

31. Cantrell DR, Inayat S, Taflove A, Ruoff RS, Troy JB. Incorporation of the electrode–electrolyte interface into finite-element models of metal microelectrodes. J Neural Eng [Internet]. 2008 Mar 1 [cited 2018 Aug 14];5(1):54–67. Available from: http://stacks.iop.org/1741-2552/5/i=1/a=006?key=crossref.c9d5638f9a5fad901b3b72c69ac1b84a

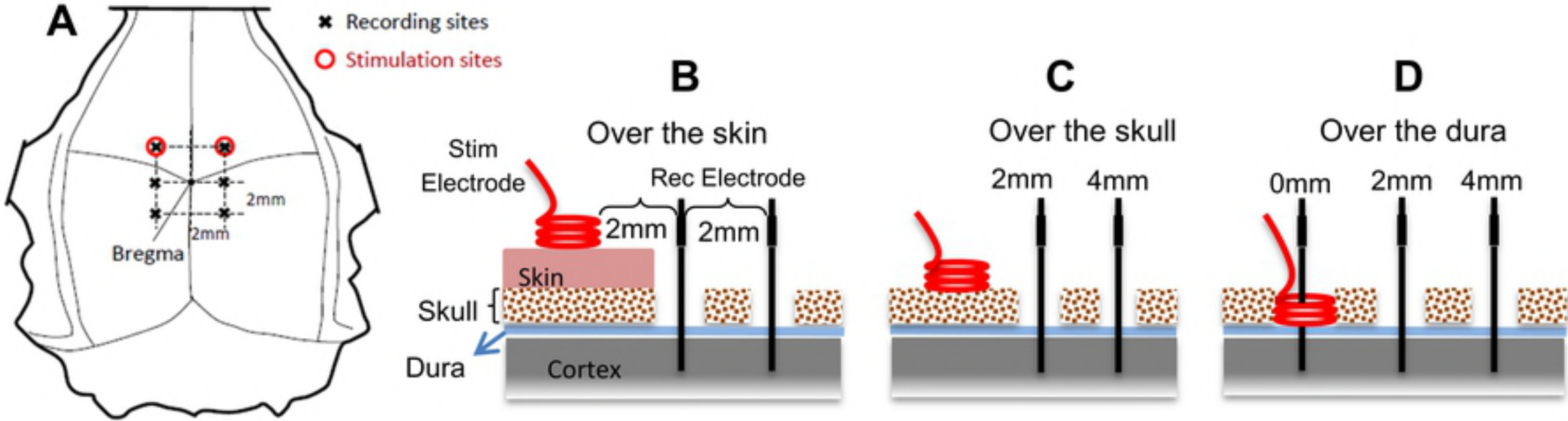
A
Recording sites
Stimulation sites
2mm
2mm
Bregma
B
Over the skin
Stim
Electrode
Rec Electrode
2mm
2mm
Skin
Skull
Dura
Cortex
C
Over the skull
2mm
4mm
D
Over the dura
0mm
2mm
4mm

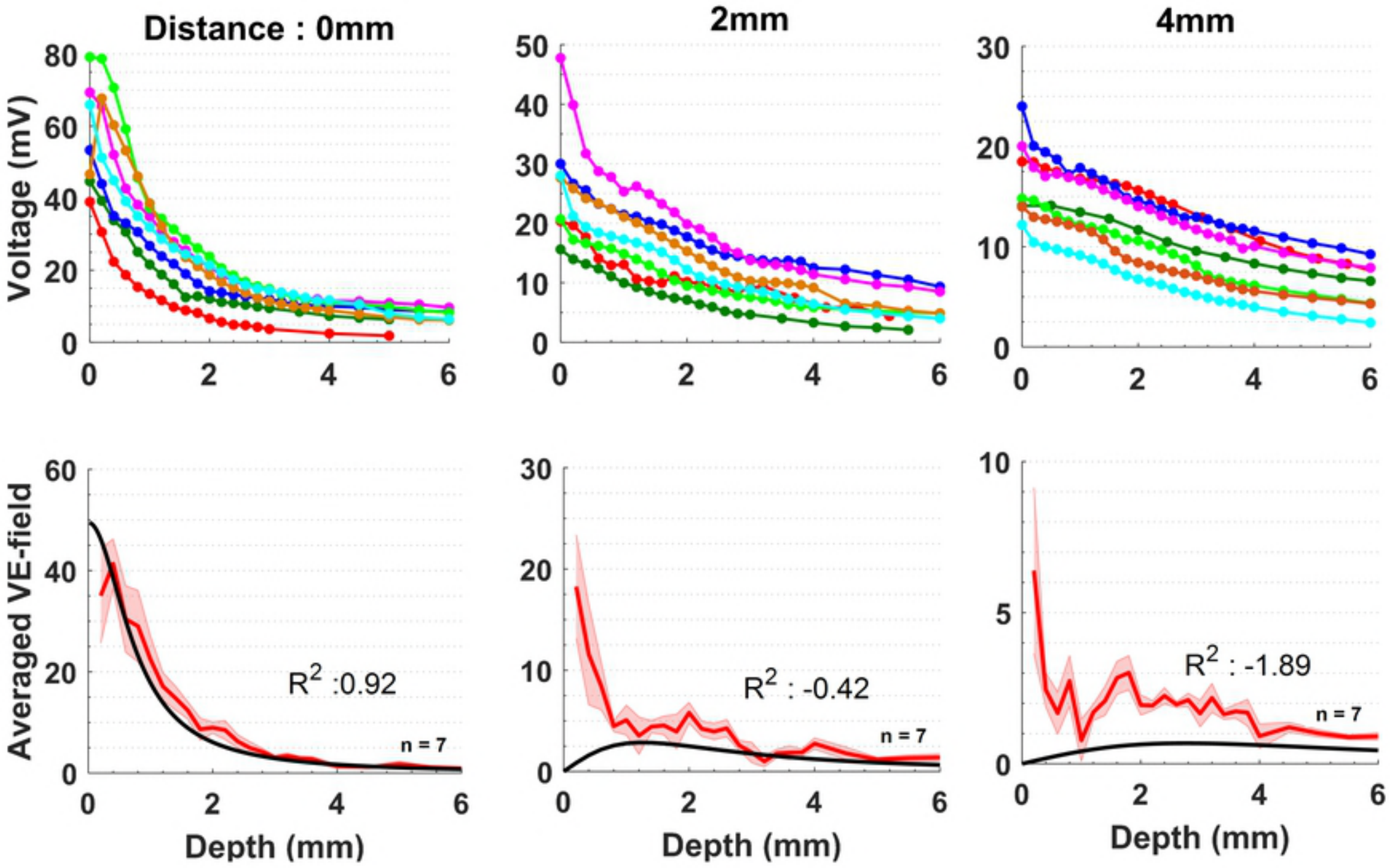
Distance : 0mm
2mm
4mm
Voltage (mV)
Averaged VE-field
Depth (mm)
Depth (mm)
Depth (mm)
R2 :0.92
R2 : -0.42
R2 : -1.89
n = 7
n = 7
n = 7

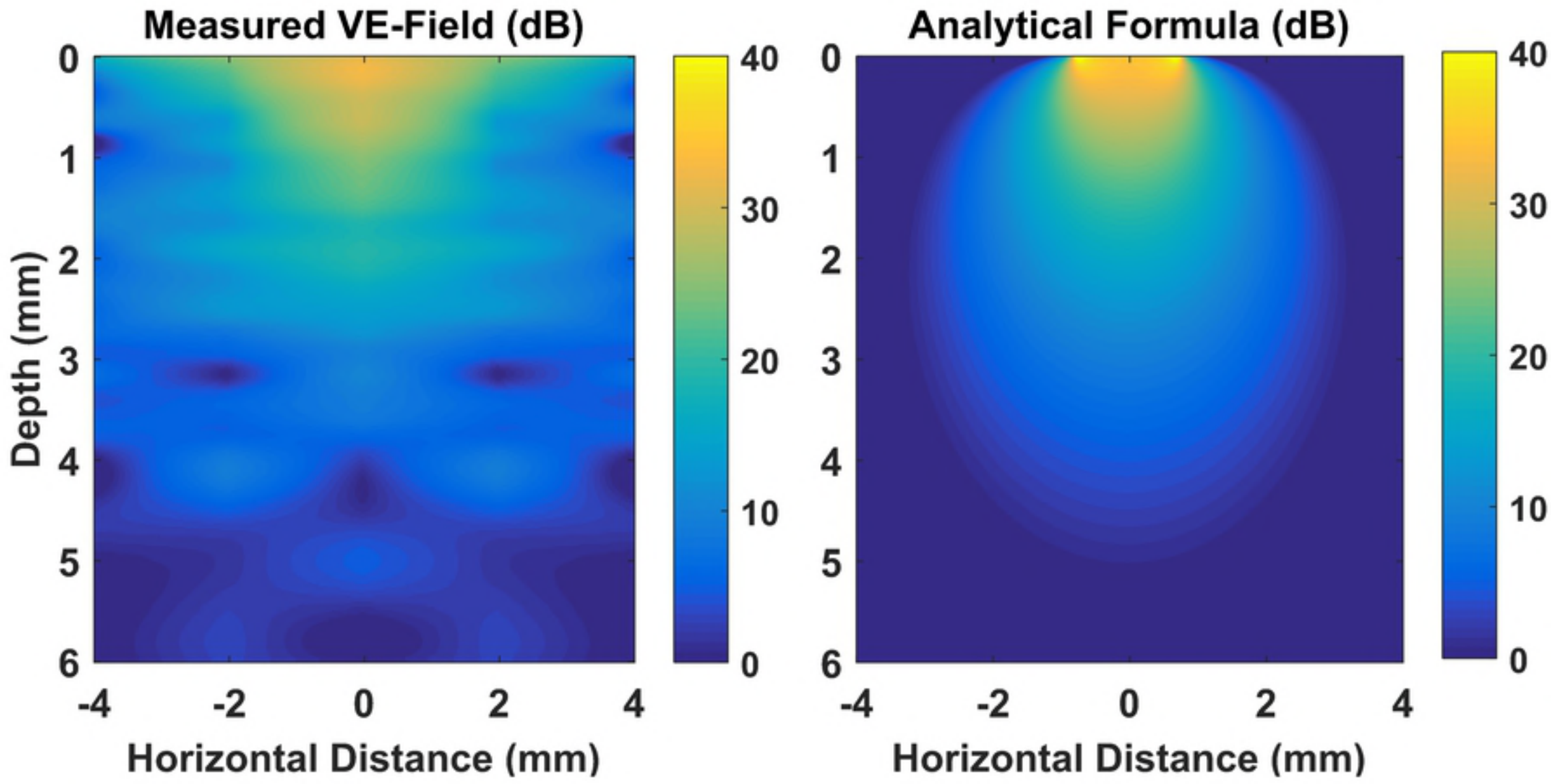
Measured VE-Field (dB)
Analytical Formula (dB)
Depth (mm)
Horizontal Distance (mm)
Horizontal Distance (mm)
0
1
2
3
4
5
6
-4
-2
0
2
4
40
30
20
10
0

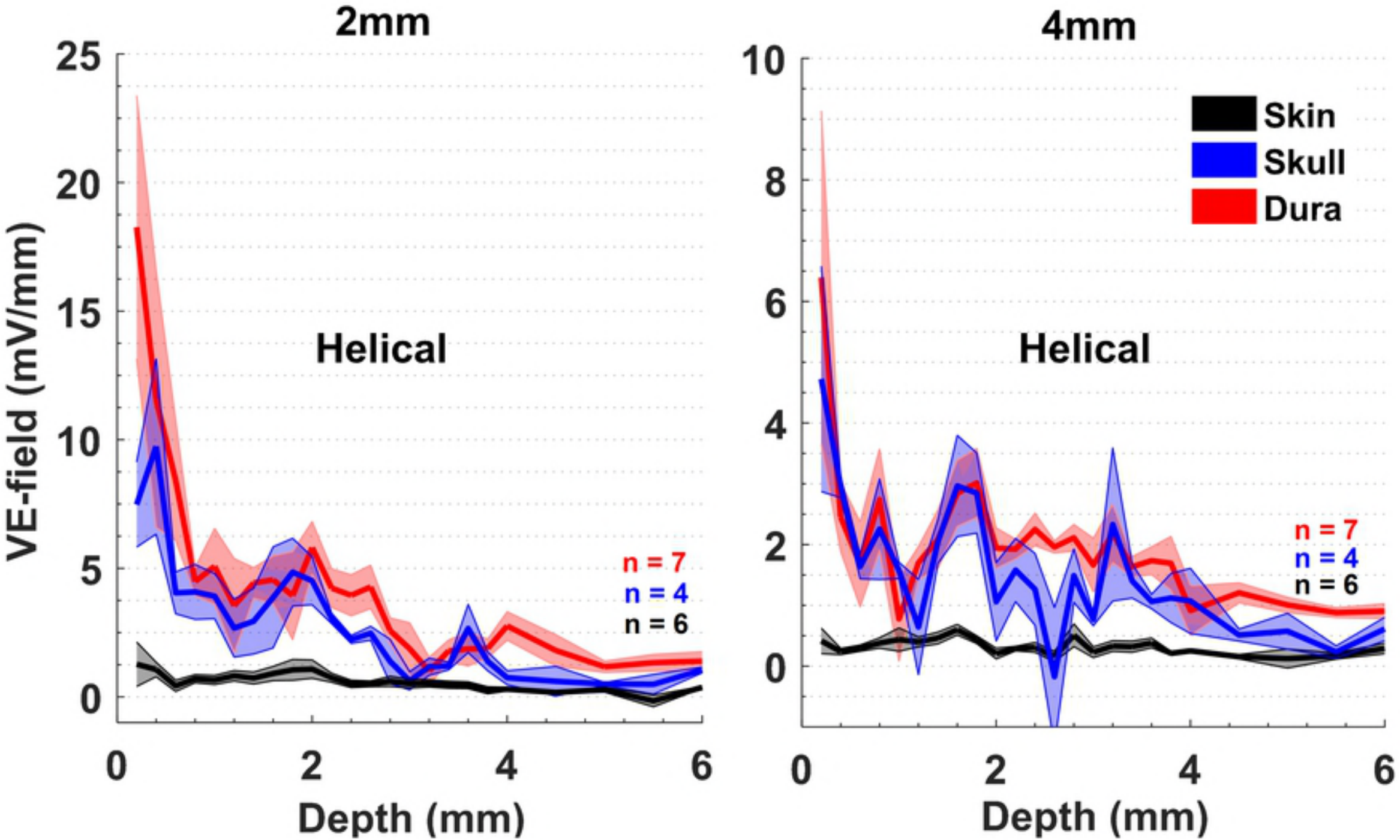
2mm
4mm
VE-field (mV/mm)
Helical
Helical
Skin
Skull
Dura
n = 7
n = 4
n = 6
n = 7
n = 4
n = 6
Depth (mm)
Depth (mm)
0
5
10
15
20
25
0
2
4
6
8
10
0
2
4
6
0
2
4
6

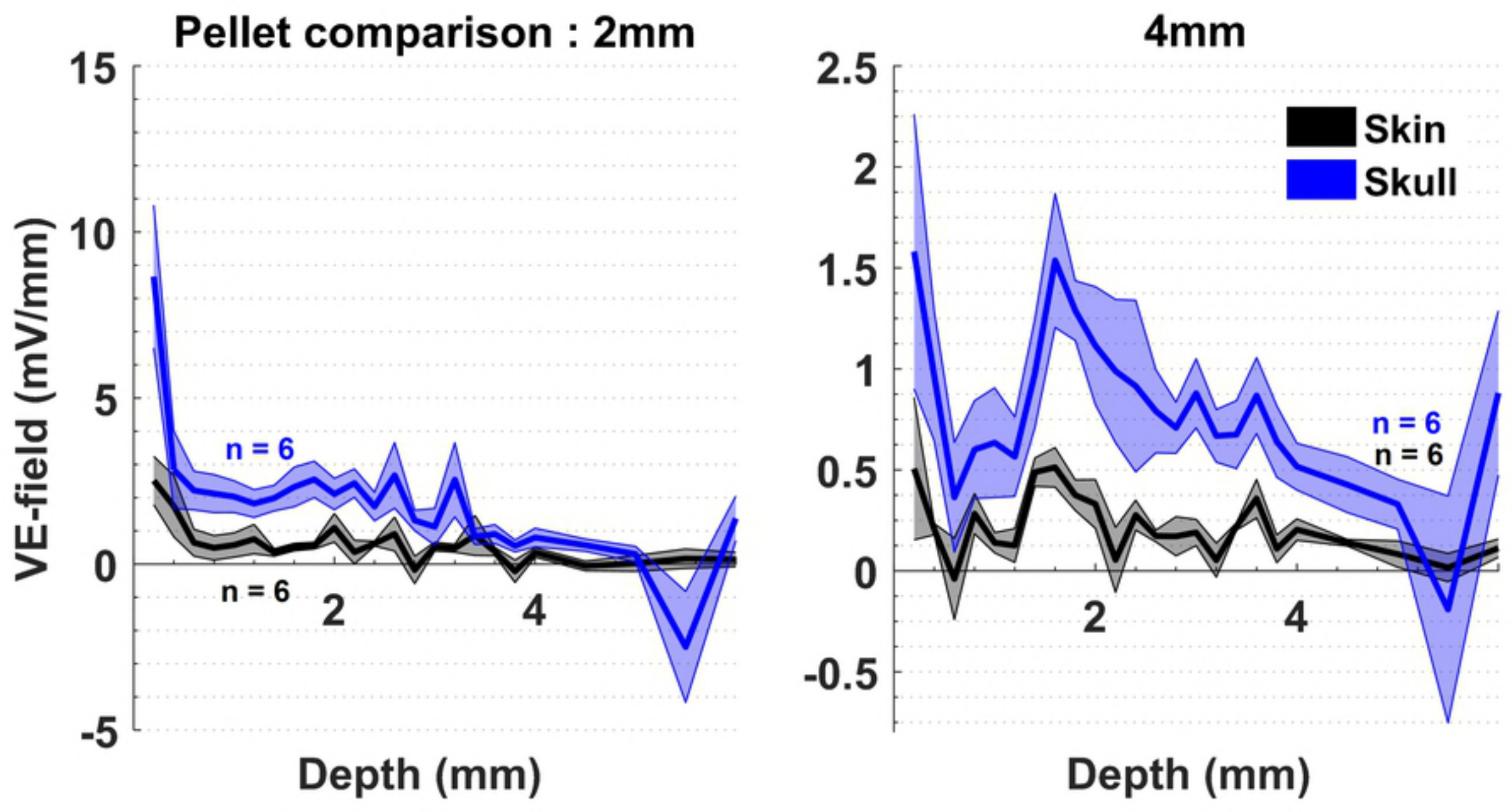
Pellet comparison : 2mm
4mm
VE-field (mV/mm)
15
10
5
0
-5
2.5
2
1.5
1
0.5
0
-0.5
Skin
Skull
n = 6
n = 6
n = 6
n = 6
2
4
2
4
Depth (mm)
Depth (mm)